Numerical Model of Fluid Flow and Oxygen Transport in a Radial-Flow Microchannel Containing Hepatocytes

G. A. Ledezma

A. Folch

S. N. Bhatia

U. J. Balis

M. L. Yarmush

M. Toner
mtoner@sbi.org

Center for Engineering in Medicine;
Surgical Services,
Massachusetts General Hospital;
Shriners Burns Hospital;
Harvard Medical School,
Boston, MA 02114

The incorporation of monolayers of cultured hepatocytes into an extracorporeal perfusion system has become a promising approach for the development of a temporary bioartificial liver (BAL) support system. In this paper we present a numerical investigation of the oxygen tension, shear stress, and pressure drop in a bioreactor for a BAL composed of plasma-perfused chambers containing monolayers of porcine hepatocytes. The chambers consist of microfabricated parallel disks with center-to-edge radial flow. The oxygen uptake rate (OUR), measured in vitro for porcine hepatocytes, was curve-fitted using Michaelis–Menten kinetics for simulation of the oxygen concentration profile. The effect of different parameters that may influence the oxygen transport inside the chambers, such as the plasma flow rate, the chamber height, the initial oxygen tension in the perfused plasma, the OUR, and K_m was investigated. We found that both the plasma flow rate and the initial oxygen tension may have an important effect upon oxygen transport. Increasing the flow rate and/or the inlet oxygen tension resulted in improved oxygen transport to cells in the radial-flow microchannels, and allowed significantly greater diameter reactor without oxygen limitation to the hepatocytes. In the range investigated in this paper ($10\ \mu m < H < 100\ \mu m$), and for a constant plasma flow rate, the chamber height, H, had a negligible effect on the oxygen transport to hepatocytes. On the contrary, it strongly affected the mechanical stress on the cells that is also crucial for the successful design of the BAL reactors. A twofold decrease in chamber height from 50 to 25 μm produced approximately a fivefold increase in maximal shear stress at the inlet of the reactor from 2 to 10 dyn/cm^2. Further decrease in chamber height resulted in shear stress values that are physiologically unrealistic. Therefore, the channel height needs to be carefully chosen in a BAL design to avoid deleterious hydrodynamic effects on hepatocytes.

Introduction

Liver failure is a major cause of morbidity and mortality. Approximately 26,000 Americans die annually from chronic liver disease and cirrhosis. In addition, more than 5000 individuals in the United States annually develop sufficiently severe hepatic failure as to require hepatic support (Yarmush et al., 1992). Unfortunately, existing nonbiological hepatic support systems are poor liver substitutes and orthotopic liver transplantation remains the only viable means for survival. Although the survival rate after liver transplantation exceeds 65 percent, many prospective recipients die while waiting for a donor due to concomitant infection or multisystem organ failure. One promising alternative is the development of an extracorporeal bioartificial liver (BAL) device. This is essentially a bioreactor containing cultured hepatocytes that function as an extracorporeal liver on a temporary basis. A BAL device could either support patients awaiting transplantation or stabilize patients during periods of hepatic regeneration recovery from fulminant hepatic failure.

To design an extracorporeal BAL device successfully with *in vitro*-cultured hepatocytes, several issues must be addressed. First, the design must provide the necessary microenvironment to hepatocytes for sustained hepatocellular functions. Second, the design must guarantee an efficient mass transport to a large number of cells in a small volume. Third, the hepatocytes should not be exposed to deleterious flow conditions such as high shear stress or pressure drop. Finally, there must be an adequate source of hepatocytes that could be a practical choice for large number of cells, and at the same time, be suitable for BAL designs targeted for animal studies and potentially for human use.

Most of the previous attempts to develop BAL devices utilize hollow-fiber cartridges originally developed for hemodialysis (Yarmush et al., 1992). Recently, two such devices have been clinically tested (Ellis et al., 1996; Watanabe et al., 1997). Despite the fact that these clinical studies showed biocompatibility of the devices, the clinical outcomes did not show significant benefits to the approaches. The reasons for this may involve the testing regimens, which have been relatively short in duration, the stability and functionality of hepatocytes in hollow fibers, and the nutrient (e.g., oxygen) and waste product transport limitations in these devices. An alternative approach using hepatocyte spheroids is also being investigated (Wu et al., 1996). However, spheroids are prone to significant diffusional limitations.

A different approach to overcome the lack of stability of cells is the use of multiplated monolayers (Uchino et al., 1988; Takahashi et al., 1992; Bader et al., 1995; Koike et al., 1996; Taguchi et al., 1996). Hepatocytes were attached to flat plates and then scaled up by using multiple layers of flat plates containing hepatocytes. Although all the animals used in these stud-

Contributed by the Bioengineering Division for publication in the JOURNAL OF BIOMECHANICAL ENGINEERING. Manuscript received by the Bioengineering Division May 28, 1998; revised manuscript received October 1, 1998. Associate Technical Editor: H. Buettner.

ies expired, the anhepatic dogs and rabbits in which the multiplated BAL devices were tested survived significantly longer than the untreated controls. One significant advantage of multiplated hepatocyte layers is the ability to seed hepatocytes onto flat plates under conditions that promote hepatocyte differentiation and function, including co-cultures (Bader et al., 1995; Koike et al., 1996) and "sandwich" cultures (Borel-Rinkes et al., 1994; Stefanovich et al., 1996; Taguchi et al., 1996). However, the critical issues concerning oxygenation of fluid flow in the design of these reactors have not been investigated. This type of theoretical information is especially important for the scaleup process.

In this study, we numerically investigate a radial-flow multiplated design for an extracorporeal BAL device consisting of cultured hepatocytes. The large aspect ratio of the microchannels proposed in our model ensures efficient oxygen transport while keeping the void volume small. The choice of radial flow as opposed to parallel flow was based on more closely mimicking the flow distribution patterns *in vivo*. Our study indicates that the oxygenation of hepatocytes in microchannels is a strong function of flow rate and inlet oxygen tension, whereas the microchannel height primarily affects the shear stress observed by hepatocytes. We also provide general criteria for the design of radial-flow multiplated BAL devices.

Bioreactor Model

The bioreactor modeled in this paper consists of several diverging-radial-flow chambers, each one formed by two parallel disks, as shown in Fig. 1. The hepatocytes are attached only on the lower disk ($z = 0$). The plasma enters at $r = R_i$ (internal radius of the disks) and exits through the edges, $r = R_e$. Thus, the cross section perpendicular to the flow increases proportionally with the radius as the flow proceeds from the center to edge. Several chambers are connected in parallel. For example, our topology utilizes stackings having a height, H, of 10 to 100 μm. The choice of a small H is allows for efficient oxygen transport while minimizing the dead volume.

Operational Parameters

In this study, we will focus on modeling and scaling of a BAL, which is capable of providing extrahepatic support for an adult rat with induced liver failure. Specifically, the BAL uses porcine hepatocytes, which have already been used in clinical trials (Ellis et al., 1996; Watanabe et al., 1997). The choice of porcine hepatocytes also complies with the BAL requirement for a large number of cells. Furthermore, we use physiological parameters that have already been used in our prior studies of extracorporeal plasma perfusion systems in rats, and oxygen consumption characteristics of porcine hepatocytes. During the simulations, these "benchmark" parameters were varied systematically to search for optimal conditions for the operation of the device.

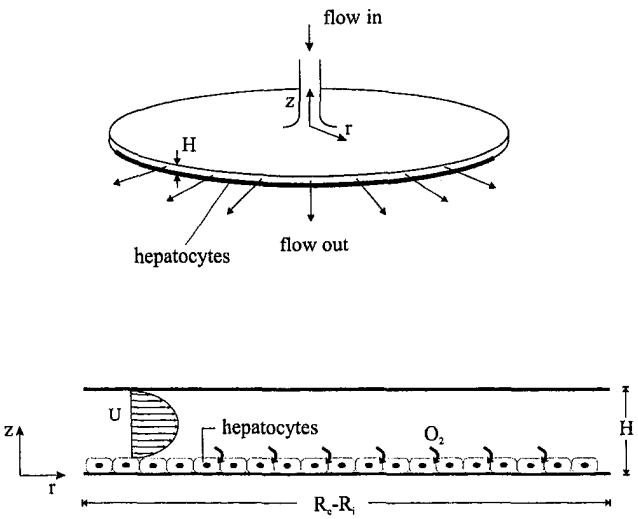

Fig. 1 Model of the BAL chambers with radial center-to-edge flow. The device scaled up in this study is composed of 10 chambers connected in parallel (piled up) with the plasma entering the chambers though the center hole (R_i = 0.3 cm).

Plasma Flow Rate. The total plasma flow rate (Q) in our extracorporeal perfusion system connected to a rat (~200 g) is approximately 0.3 mL/min as reported by Stefanovich et al. (1996). This represents approximately 25 percent of the rat's arterial output that enters the plasma separator.

Oxygen Consumption. The bioreactor presented in this study is based on a strategy of pre-seeding (attached/spread) cells. By using such approach, the necessity of maintaining the hepatocyte's viability throughout the critical initial phases of culture is avoided (Balis et al., 1998). Furthermore, the high initial values of V_{max} (maximal OUR) can be ignored if the pre-seeded bioreactor chambers are incorporated in the BAL after the eighth day of culture. As a result, we use a typical average post-seeding value of V_{max}, specifically after the eighth day of culture (V_{max} = 0.25 nmoles O_2/s/10^6 cells). Previous studies have also shown that the OUR versus oxygen tension behavior of both rat and porcine hepatocytes follow very closely a first-order Michaelis–Menten process (Foy et al., 1994; Balis et al., 1998). Therefore, in order to model the OUR of the hepatocytes accurately, we used Michaelis–Menten kinetics. This model, depicted in Eq. (11), requires the knowledge of the oxygen partial pressure at which the OUR is half-maximal (K_m). We used K_m = 5 mmHg, which is an average of the values reported by Balis et al. (1998) after the eighth day of culture.

Cell Mass Estimation. An adult rat liver has approximately 350 million hepatocytes (Stefanovich et al., 1996). It has been estimated that the minimal fraction of liver mass necessary for survival ranges between 2 and 12 percent. (Demetriou et al., 1988; Asonuma et al., 1992). Therefore, we chose an intermediate value, namely, 6 percent, of the total number of hepatocytes in the liver. This estimate gives a total of 20 million hepatocytes in the BAL, necessary to support the rat.

Oxygen Tension. It has been postulated that the partial pressure of oxygen may have an important role in urea synthesis, lipid metabolism, cytochrome P-450 activity and gluconeogenesis both *in vivo* and *in vitro* (Bhatia et al., 1996). These specific liver functions are known to be localized within a specific zone of the sinusoidal endothelium, where the oxygen tension ranges between 90 and 5 mmHg. As a consequence, the preservation of the hepatocyte functions in a BAL may be achieved by exposing the hepatocytes to an oxygen tension gradient similar to the one observed *in vivo*. In our simulations we varied the oxygen tension between 380 mmHg (50 percent oxygen dissolved in plasma) at the inlet and 5 mmHg at the outlet. The choice of 5 mmHg as the cut-off value was based on the physiological range as stated above and corresponded fortuitously to K_m of porcine hepatocytes. The actual minimal (cutoff) oxygen tension may be different from our estimation and needs to be investigated experimentally. Although the inlet oxygen tension in our BAL chambers is higher than values observed *in vivo*, we choose a high oxygen tension to achieve chamber length sufficiently long to accommodate a large number of hepatocytes.

Dead Volume. There is a limitation in the total volume of fluid that can be contained inside the BAL. A large dead volume (the total volume of the BAL device and extracorporeal interconnects) would cause dilution of the BAL products. The bioactivity of these compounds relies on a minimal critical con-

centration; therefore, dilution would compromise device performance. In our study, the maximal allowable dead volume of the BAL is taken as 3 mL. It represents roughly 30 percent of the total rat blood volume (Bhatia et al., 1994). Approximately 1 mL should be allocated for the volume occupied by the chambers, and the remaining for tubing, interconnects and the volume inside the BAL housing itself.

Cell Density. Both porcine and rat hepatocytes have been typically seeded at 100,000 cells/cm^2 for experimental measurement of OUR (Rotem et al., 1992; Balis et al., 1998). Since our simulations use V_{max} and K_m data from Balis et al. (1998), we used the same cell density for consistency. Simulations were performed using different hepatocyte densities ranging from 50,000 to 200,000 cells/cm^2 and demonstrated no significant difference in the total cell number without oxygen limitation.

Shear Stress and Pressure Drop. The hepatocytes in the BAL will be subjected to a mechanical stress that might have detrimental effects on their function and viability. We used a conservative threshold shear stress of 10 dyne/cm^2, based on the orders of magnitude exhibited in earlier studies using endothelial cells (Frangos et al., 1988). In addition, typical *in vivo* values of pressure drop are used as an upper limit in our calculations. For example, Nakata et al. (1960) report a pressure drop between 1.5 and 9 mmHg from the portal vein to the hepatic vein. As a result, we chose a conservative value of 8 mmHg ($\sim$10,000 dynes/cm^2).

We based our study on a bioreactor composed of 10 chambers as the one shown in Fig. 1. We chose 10 chambers as a first approach in order to utilize a multichamber modular design. Furthermore, a pilot bioreactor could be easily constructed to validate the predictions of the model experimentally and further to investigate the metabolic output of the cells during operation conditions. Each chamber had an internal radius, R_i = 0.3 cm, and a height, H = 50 μm. These dimensions provided an efficient distribution of the plasma among the chambers and minimized the dead volume. Using these parameters, we found that we would need a total of 2 million seeded hepatocytes on each chamber, with an external diameter, $R_e \approx$ 2.55 cm, in order to comply with the 20 million hepatocytes requirement.

Numerical Method

The numerical simulations were developed in a two-dimensional domain such as the one outlined on the bottom of Fig. 1. The flow is two dimensional because it is independent of the angular coordinate (i.e., axisymmetric). Our model was simplified by assuming that the flow originated at a segment of the axis of symmetry, r = 0. In other words, the possible transitions between axial and radial flow were neglected.

The set of dimensionless conservation equations for mass, momentum and species (oxygen) that correspond to the configuration shown in Fig. 1 are:

$$\frac{\partial \tilde{v}_r}{\partial \tilde{r}} + \frac{\tilde{v}_r}{\tilde{r}} + \frac{\partial \tilde{v}_z}{\partial \tilde{z}} = 0 \tag{1}$$

$$\tilde{v}_r \frac{\partial \tilde{v}_r}{\partial \tilde{r}} + \tilde{v}_z \frac{\partial \tilde{v}_r}{\partial \tilde{z}} = -\frac{\partial \tilde{p}}{\partial \tilde{r}} + \frac{1}{\mathrm{Re_D}}\left(\frac{\partial^2 \tilde{v}_r}{\partial \tilde{r}^2} + \frac{1}{\tilde{r}}\frac{\partial \tilde{v}_r}{\partial \tilde{r}} - \frac{\tilde{v}_r}{\tilde{r}^2} + \frac{\partial^2 \tilde{v}_r}{\partial \tilde{z}^2}\right) \tag{2}$$

$$\tilde{v}_r \frac{\partial \tilde{v}_z}{\partial \tilde{r}} + \tilde{v}_z \frac{\partial \tilde{v}_z}{\partial \tilde{z}} = -\frac{\partial \tilde{p}}{\partial \tilde{z}} + \frac{1}{\mathrm{Re_D}}\left(\frac{\partial^2 \tilde{v}_z}{\partial \tilde{r}^2} + \frac{1}{\tilde{r}}\frac{\partial \tilde{v}_z}{\partial \tilde{r}} + \frac{\partial^2 \tilde{v}_z}{\partial \tilde{z}^2}\right) \tag{3}$$

$$\tilde{v}_r \frac{\partial \tilde{C}}{\partial \tilde{r}} + \tilde{v}_z \frac{\partial \tilde{C}}{\partial \tilde{z}} = \frac{1}{\mathrm{Re_D\ Sc}}\left[\frac{1}{\tilde{r}}\frac{\partial}{\partial \tilde{r}}\left(\tilde{r}\frac{\partial \tilde{C}}{\partial \tilde{r}}\right) + \frac{\partial^2 \tilde{C}}{\partial \tilde{z}^2}\right] \tag{4}$$

where Eqs. (2) and (3) are the Navier–Stokes equations of fluid motion at steady state assuming nearly constant properties evaluated at 37°C. Equations (2) and (3) were simplified neglecting the inertial terms, and the resulting linear equations (Stokes flow equations) were solved first to obtain the velocity field. Later, the velocities were substituted into Eq. (4), which had to be solved iteratively.

The Stokes flow assumption can be justified using scale analysis. In our geometric configuration depicted in Fig. 1, $H \ll (R_e - R_i)$. This geometric feature combined with Eq. (1) provides the order of magnitude of the velocities,

$$V_z \sim \frac{H}{(R_e - R_i)} V_r \sim 0 \tag{5}$$

Similarly, the momentum equation in r can be written in an order of magnitude sense,

$$\rho \frac{V_r^2}{(R_e - R_i)}, \frac{H}{(R_e - R_i)} V_r^2 \sim \frac{p}{(R_e - R_i)}, \mu \frac{V_r}{(R_e - R_i)^2}, \frac{V_r}{H^2} \tag{6}$$

where only the first term of the left-hand side and the first and last terms of the right-hand side survive the scaling process, due to the V_z scale [Eq. (5)], and the slenderness of our chambers [$H \ll (R_e - R_i)$]. Therefore, Eq. (6) becomes,

$$\mathrm{Re_D} \frac{V_r}{2H(R_e - R_i)} \sim \frac{p}{\nu(R_e - R_i)}, \frac{V_r}{H^2} \tag{7}$$

where the left-hand side is the scale of the inertia and the right-hand side furnishes the scales of the pressure difference across the chamber and friction. The pressure term must not vanish because it is the driving force of the flow. However, comparing the scales of the inertia and friction, we conclude that the first must be negligible because $\mathrm{Re_D}$ has an order of magnitude smaller than 1,

$$\frac{\mathrm{Re_D}}{2(R_e - R_i)} \ll \frac{1}{H} \tag{8}$$

A more direct approach to evaluate the importance of the inertial terms in a radial flow configuration is provided by Goldstein and DiMilla (1997). They showed that the Stokes (creeping) flow solution is reasonable in radial positions given by

$$r > \left(\frac{2|Q|H}{7\pi\nu}\right)^{0.5} \tag{9}$$

If the parameters that correspond to our design (Q = 0.0167 cm^3/s, H = 0.005 cm, and ν = 0.01 cm^2/s) are substituted into Eq. (9), we find that $r > 0.27$ mm. Since our internal radius is 3 mm, we conclude that Stokes flow is, in fact, a very good "approximation" in our model.

The nondimensional variables used for writing Eqs. (1)–(4) are:

$$(\tilde{r}, \tilde{z}) = \frac{(r, z)}{D_h} \quad (\tilde{v}_r, \tilde{v}_z) = \frac{(v_r, v_z)}{U} \tag{10}$$

$$\tilde{p} = \frac{p}{U^2\rho} \quad \tilde{C} = \frac{C}{C_i} \tag{11}$$

$$\mathrm{Re_D} = \frac{UD_h}{\nu} \quad \mathrm{Sc} = \frac{\nu}{D} \tag{12}$$

where Sc is the Schmidt number, $\mathrm{Re_D}$ is the Reynolds number based on the hydraulic diameter, ν is the kinematic viscosity, $\nu = \mu/\rho$ = 0.01 cm^2/s as reported by Frangos et al. (1988), C

is the oxygen concentration, C_i is the inlet oxygen concentration, D_h is the hydraulic diameter ($D_h = 2H$), U is the mean velocity at the inlet ($r = R_i$), p is the pressure, D is the diffusivity of oxygen in plasma (2×10^{-5} cm^2/s), and ρ is the density of the fluid. It is worth mentioning that lower values for the kinematic viscosity have been reported by other investigators. Truskey and Pirone (1990), for example, reported $\nu = 0.0084$ cm^2/s at 37°C. We intentionally picked the largest possible viscosity to obtain conservative values of shear stress.

We conducted our numerical work in a two-dimensional computational domain represented by one chamber $[(R_e - R_i) \times H]$ fitted with a downstream section ($L_d \times H$) (Ledezma and Bejan, 1997). This allowed us to impose appropriate outflow boundary conditions [Eq. (15)]. L_d was chosen based on accuracy tests described later in this section. Its dimensionless value was $L_d/L = 0.05$.

The flow boundary conditions are: uniform horizontal velocity at the channel inlet; no slip and no penetration on the walls of the channel; and zero shear at the outlet. In addition, the boundary conditions for Eq. (4) are:

$$\check{C} = \check{C}_0 \quad \text{at} \quad \check{r} = 0 \tag{13}$$

$$\frac{\partial \check{C}}{\partial \check{z}} = 0 \quad \text{at} \quad \check{z} = \check{h} \tag{14}$$

$$\frac{\partial \check{C}}{\partial \check{r}} = 0 \quad \text{at} \quad \check{r} = \check{L} \tag{15}$$

The boundary condition at $\check{z} = 0$ is the OUR of the hepatocytes. It is not constant because cells adapt to depletion of oxygen by reducing their OUR. Hence, the oxygen concentration profile $C(r, z)$ in the chamber is a function of the oxygen concentration at the surface with attached cells, $C_s(r)$. Using Michaelis–Menten kinetics (Britton, 1986) the OUR of the hepatocytes is modeled as:

$$D\left(\frac{\partial C(r, z)}{\partial z}\right)_{z=0} = V_{\max} \frac{C_s(r)}{K_m + C_s(r)} \tag{16}$$

Equations (1)–(4) were solved using a Galerkin finite element code (FIDAP, 1993) and a sufficiently fine grid with quadrilateral elements and biquadratic interpolating functions for the velocities and oxygen concentration. The pressure was eliminated using the penalty formulation and reduced integration (Reddy and Gartling, 1994) with a penalty parameter $\epsilon = 10^{-8}$. As previously described (Ledezma and Bejan, 1997), we verified that our results are nearly insensitive to the penalty parameter. An attenuation factor of 0.5 was applied to all the degrees of freedom to maintain the convergence under control. The convergence for the species equation, Eq. (4), took roughly between 40 and 60 Broyden (quasi-Newton) iterations. We used the following criteria to stop the simulations (FIDAP, 1993):

$$\frac{\|\Delta u_i\|}{\|u\|} \leq 10^{-3} \quad \text{and} \quad \frac{\|R(u_i)\|}{\|R_0\|} \leq 10^{-3} \tag{17}$$

where $\|\cdot\|$ is the Euclidean norm, u_i is the solution vector at iteration i, and $R(u_i)$ is the residual vector.

The mesh was uniform in r with 401 nodes and nonuniform in z with between 29 and 37 nodes. Accuracy tests showed that the solutions are mesh independent. The grid fineness was increased until the relative changes on the integrated mean oxygen concentration in all the computational domain was less than 0.1 percent when the number of nodes was increased by 25 percent in each direction. Another set of accuracy tests indicated that the integrated mean oxygen concentration was relatively insensitive to doubling of the downstream length (L_d) of the computational domain.

Oxygen Transport Within the Bioreactor Chambers

There is functional evidence that low oxygen tension *in vitro* decreases viability and function of hepatocytes (Bhatia et al., 1996). This mandates that the hepatocyte-seeded surface be efficiently oxygenated. In this section, we modeled the constraints on BAL dimensions and flow conditions imposed by the oxygen consumption of hepatocytes inside the perfusion chamber of Fig. 1. The objective was to find the optimal plasma flow rate needed to perfuse 20 million hepatocytes in the bioreactor at a minimal acceptable oxygen tension of $K_m^* = 5$ mmHg as stated above. In addition, we carried out a sensitivity analysis (depicted in Fig. 5) and concluded that higher values of K_m^* do not significantly decrease the total number of cells that are successfully perfused within the chambers. In the following sections of the paper, we systematically varied other parameters to study their individual impact upon oxygen transport.

A. The Effect of the Plasma Flow Rate. We define the achievable chamber radius or critical radius, R_c, as the radius at which the oxygen tension at the surface with attached hepatocytes is equal to K_m^*. Figure 2 depicts R_c as a function of the total plasma flow rate in the bioreactor. Higher plasma flow rates provide a larger R_c and more cells exposed to oxygen tensions above K_m^* due to the increase in oxygen convection. Moreover, in order to utilize 20 million hepatocytes ($R_c = 2.55$ cm, when cells are seeded at 10^5 cells/cm^2) with an oxygen tension above K_m^*, we needed to ensure that $Q \approx 1$ mL/min; thus, each chamber required perfusion with plasma at 0.1 mL/min or greater. This plasma flow rate is three times higher than previously reported by Stefanovich et al. (1996). The threefold increase in Q was achievable because the separated plasma circulated in a semi-independent circuit and it was later recombined with the arterial blood in the external circuit, where flow was approximately 1.2 mL/min.

Figure 3 illustrates the oxygen concentration patterns along the chamber. The height of the chamber has been intentionally expanded to display the oxygen profile in greater detail. From the oxygen gradients, we can assess the impact of the Reynolds number (plasma flow rate, $\mathrm{Re_D} = Q/\pi R_i \nu$) upon cell viability. The region of the chamber with high oxygen tension extends further downstream as the Reynolds number increases. Thus, in the chamber depicted on the top of Fig. 3, the diffusion of oxygen is the dominating transport mechanism. The pattern of the chamber depicted on the bottom of Fig. 3 represents a convection-dominated transport of oxygen. The darkest regions of the chamber are those with very low oxygen tension where the hepatocytes are thought to become ischemic. These results strengthen the conclusion reached in Fig. 2, namely that higher plasma flow rates (faster circulation of the plasma in the chambers) increase the levels of oxygen concentration in the plasma.

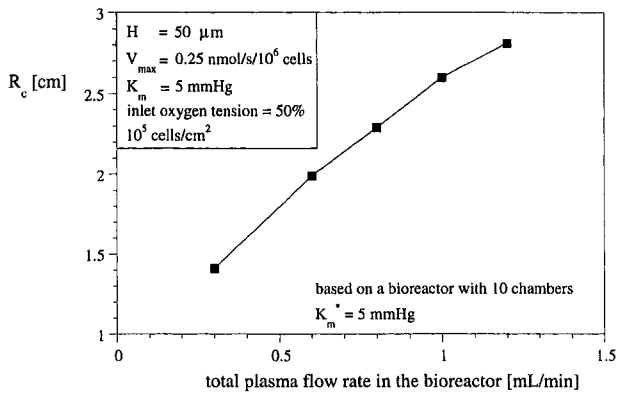

Fig. 2 The critical radius as a function of the total plasma flow rate in a bioreactor with 10 chambers. Each chamber has a plasma flow rate equal to 0.1 mL/min.

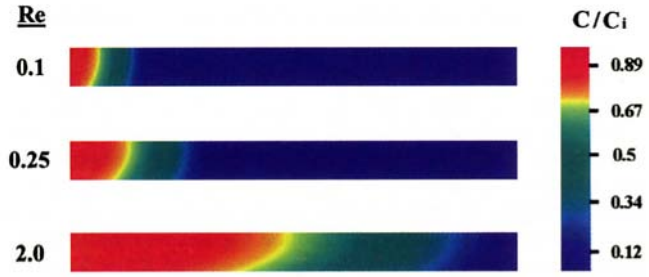

Fig. 3 The two-dimensional oxygen concentration profile in a plasma-perfused chamber. The flow conditions are V_{max} = 0.4 nmol/s/10^6 cells, K_m = 5 mmHg, H = 100 μm, and 10^5 cells/cm^2. The Reynolds number is defined as $Re_D = Q/\pi R_i \nu$.

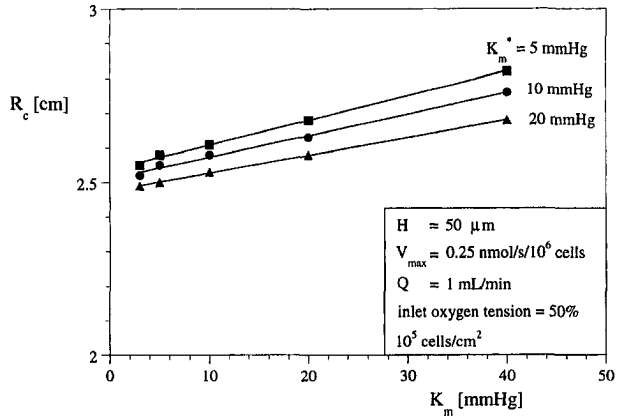

Fig. 5 The effect of K_m on the critical radius of the BAL chambers. The critical radius was calculated using three values of K_m^* (minimal allowed oxygen tension in the chambers).

B. Sensitivity of the Model to the OUR Parameters, V_{max} and K_m. V_{max} and K_m are experimentally determined variables subject to variability depending on the duration of culture, and cell microenvironment. As a result, the effect of varying V_{max} and K_m needed to be investigated. Although these parameters cannot typically be manipulated or changed via design of the BAL, it is critical to define the sensitivity of our model to these parameters.

The total plasma flow rate in the BAL is kept constant at 1 mL/min because it has already been found in Fig. 2 that such Q can maintain a BAL with 10 chambers having $R_c = R_e$ = 2.55 cm (20 million cells perfused with plasma above K_m^*). In Fig. 4, V_{max} is varied from 0.2 to 0.4 nmol/s/10^6 cells, because these values bracket our experimentally determined baseline V_{max} of 0.25 nmoles/s/10^6 after 8 days of hepatocyte culture. The values depicted in the abscissa represent the oxygen tension at the surface of the chamber with attached hepatocytes, normalized with respect to the inlet oxygen tension. Perturbations in V_{max} have a dramatic effect on reactor design. The critical radius increases from 2.1 cm when V_{max} = 0.4 nmol/s/10^6 cells, to 2.9 cm when V_{max} = 0.2 nmol/s/10^6 cells, corresponding to an increase in viable cell number from 13.5 to 26.1 million.

The sensitivity of the oxygen profile to variations in K_m is shown in Fig. 5. The abscissa depicts the critical radius for different values of K_m^*. The variation in R_c between 2.5 and 2.8 cm only makes the number of hepatocytes operating above K_m^* increase from 19.3 million to 24.3 million. The fact that R_c is almost insensitive to K_m becomes clearer if we choose as a minimum (cut-off) oxygen tension K_m itself, in other words, $K_m^* = K_m$. Reading R_c from Fig. 5 we conclude that in the range $5 < K_m < 20$ mmHg, R_c will always be close to 2.55 cm.

C. Oxygen Tension at the Inlet of the Chambers. The plasma can be easily oxygenated in the extracorporeal circuit by either incorporating a membrane oxygenator or through the use of gas permeable tubing. Although oxygen tension is a potentially well-regulated factor in the BAL design, few aspects should be taken into account before choosing an inlet oxygen tension for the operation of the BAL. Increases in inlet oxygen tension will increase the number of hepatocytes that are exposed to oxygen tensions above K_m^*. While it is not clear whether high oxygen tensions could negatively impact cells, it is hypothesized that high levels of oxygen may cause oxidative damage by the formation of free radicals. Therefore, the highest oxygen tension at the chamber inlet should be limited to that required to achieve our desired chamber length with all hepatocytes being maintained above K_m^*.

We studied the oxygen tension range between 10–60 percent (76–456 mmHg) at the inlet of the chambers. Figure 6 shows the increase in the critical radius as the inlet oxygen tension becomes higher. For example, if room air was used to oxygenate the plasma, the critical radius would be approximately 1.6 cm (~7.8 million hepatocytes above K_m^*). However, if the inlet oxygen tension was increased to 60 percent, the total number of hepatocytes above K_m^* would be nearly 23 million. This threefold increase in hepatocyte number suggests that the initial oxygen tension is an excellent regulator of the oxygen distribution within the BAL chambers.

Since we required an inlet oxygen tension of 380 mmHg to obtain 20 million viable cells (R_c = 2.55 in Fig. 6), the possibil-

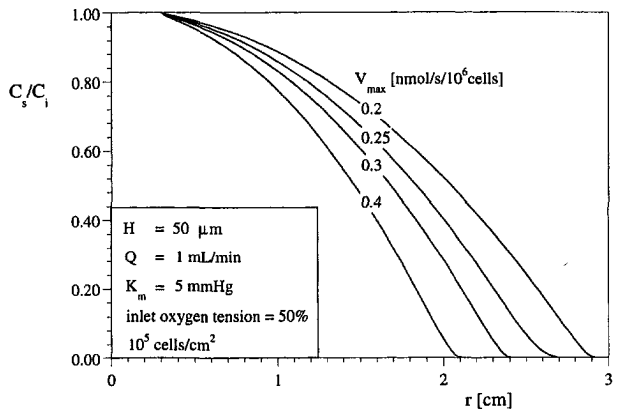

Fig. 4 The effect of the maximal oxygen uptake rate (V_{max}) on the dimensionless oxygen concentration at the cell-seeded surface of the BAL chambers

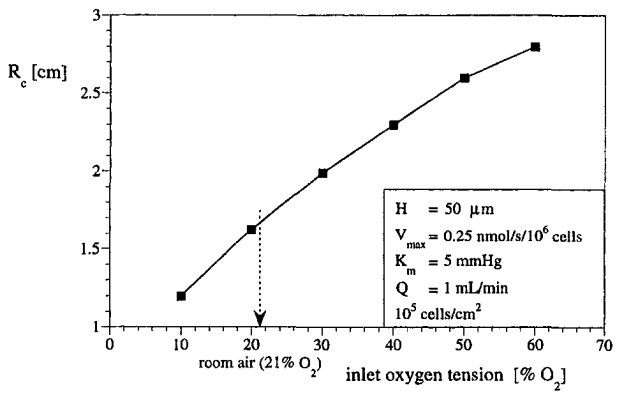

Fig. 6 The effect of the inlet oxygen tension on the critical radius. The critical radius was calculated using a minimal allowed oxygen tension, K_m^* = 5 mmHg.

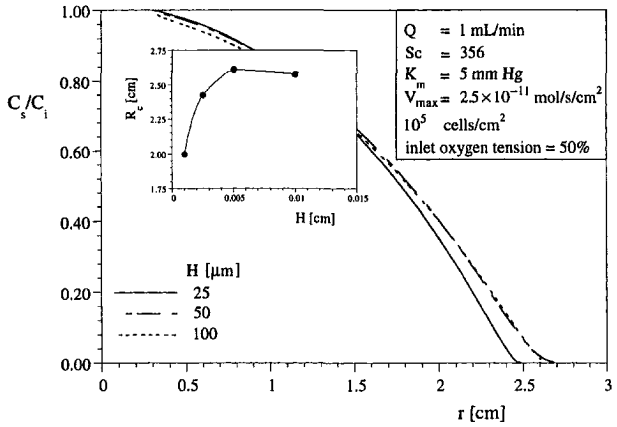

Fig. 7 The effect of the channel height on the oxygen concentration at the chamber surface with attached hepatocytes ($z = 0$). The inset shows the critical radius, R_c, where the hepatocytes are exposed to an oxygen tension, $K_m^* = 5$ mmHg.

ity of oxidative damage became an important issue warranting further experimental investigation. Previous studies have only addressed the effect of varying oxygen tension in hepatocyte function in the early stages of culture. For example, Foy et al. (1994) have shown that hepatocytes do not suffer from deleterious effects at these tensions. Rather, the attachment of the hepatocytes in microcarriers improves when the oxygen partial pressures are 50 percent or higher, suggesting there may be some benefit to operating in these range *in vitro*. However, these results should not be directly extrapolated to our model because the hepatocytes in the BAL topology we studied were already 8 days old. For long time intervals, exposure to elevated oxygen tensions may cause some cumulative oxidative damage.

D. The Effect of the Chamber Height. We studied the influence of H on the oxygen tension under a constant plasma flow rate of 1 mL/min (0.1 mL/min perfused to each chamber). Figure 7 depicts the dimensionless oxygen concentration profile at the surface with cells. The results show that H has a weak effect on the oxygen concentration profile at the surface with attached cells. It is worth noting that R_c has a shallow maximum at $H \sim 50$ μm (shown as an inset in Fig. 7). This can be explained with the asymptotic behavior of the oxygen transport. When H is large, the flow velocity becomes very slow and the oxygen transport is diffusion limited. In the other extreme, when H is small, the flow velocity becomes large but the plasma volume vanishes as does the oxygen.

These results have several implications. First, in the range studied in this paper, the height of the chambers will not play an important role in the efficiency of the oxygen transport. However, it imposes a constraint when keeping the dead volume of the BAL small. On the other hand, H does have an important effect on both the shear stress and the pressure drop inside the bioreactor chambers. We study these hydrodynamic issues in the next section of the paper.

Shear Stress and Pressure Drop

In this section we study the constraints in the BAL design imposed by the hydrodynamics of the plasma flow within the chambers. To unveil the most important parameter affecting both the shear stress and pressure drop, we use the solution for creeping flow between to parallel plates with radial flow:

$$\tau_w = \frac{3\mu Q}{\pi H^2 r} \tag{18}$$

where τ_w is the shear stress. Similarly, the pressure drop is also inversely proportional to the chamber height, $\Delta P \sim 1/H^3$. As a result, the variation of the shear stress and pressure drop in the chambers will be strongly affected by H.

The shear stress at the lower disc is obtained from the numerical results as:

$$\tau = \tau_{rz} = -\mu \frac{\partial v_r}{\partial z} \tag{19}$$

Additionally, the pressure solution is recovered from the formulation of the penalty function:

$$\frac{\partial v_r}{\partial r} + \frac{V_r}{r} + \frac{\partial v_z}{\partial z} = -\epsilon p \tag{20}$$

Figure 8 depicts both the pressure drop and shear stress as a function of the chamber radius for four different values of H. The plasma flow rate in the bioreactor is 1 mL/min (0.1 mL/min in each chamber). In addition, the pressure drop values are based on a chamber with $R_c = 2.5$ cm. The predictions of Eq. (18) are corroborated by the curves shown in Fig. 8. Furthermore, the agreement between the numerical solutions and Eq. (18) is excellent. Reducing the chamber height from 50 to 25 μm produces an increase from roughly 2 to 10 dyne/cm^2 in the maximal shear stress, which occurs at the inlet of the chamber. A similar steep change can be observed in the pressure drop across the chamber. When H is lower than 25 μm the pressure drop becomes higher than 10,000 dyne/cm^2 and the hepatocytes can be negatively affected. The shear stress when H is lower than 25 μm is also unacceptable.

In brief, observing the effect of H on the oxygen transport (inset of Fig. 7) and hydrodynamics, we can choose H to be between 25 and 50 μm. If we use 50 μm, for example, the contribution of the chambers to the dead volume is only 1 mL, leaving 2 mL for additional space in the bioreactor.

Conclusions

In this paper we examined the fundamental elements that govern the design of a modular BAL, which incorporates diverging-radial-flow microfabricated chambers with monolayers of porcine hepatocytes and perfused plasma, using oxygen uptake as an indicator of metabolic measurements. We constructed a numerical model and generated BAL design and scale-up data for hypothesized physiological conditions within an adult rat. We have unified several experimental and theoretical findings from previous reports to propose a design in which mass transport limitations and mechanical stress damage to cells is mini-

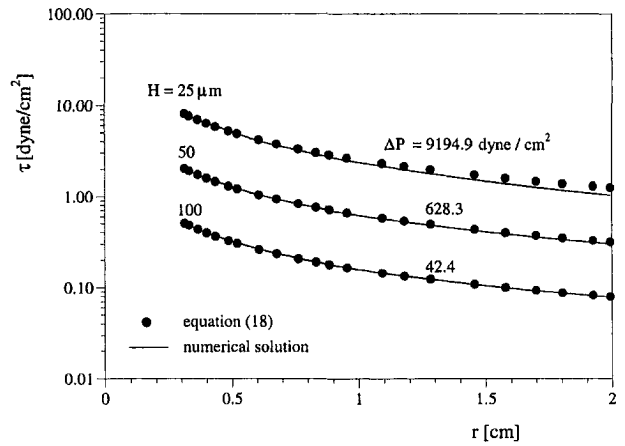

Fig. 8 The effect of the chamber height on the shear stress and pressure drop. The total plasma flow rate is fixed, $Q = 1$ mL/min (0.1 mL/min per chamber). The pressure drop is calculated using a chamber radius equal to 2.5 cm.

mized. The two parameters that influenced the oxygenation of hepatocytes in microchannels are found to be the flow rate and the inlet oxygen tension. By increasing and adjusting these two parameters, the adequate oxygenation of all hepatocytes in the BAL device can be satisfied. The other key factor was the height of the flow chambers. Despite the fact that the channel height had minimal effect on the oxygenation of hepatocytes, it strongly influenced the shear stress to which hepatocytes were exposed during flow. Channel heights in the range of 25 to 50 μm resulted in reasonable shear stress values; however, further decrease in channel height caused dramatic increase in shear stress to values several orders of magnitude above the physiological range. We have utilized physiological parameters determined both *in vivo* and *in vitro* to allow us to mimic the true operation conditions as closely as possible. This approach could be extended to more complex geometric configurations. Future work will allow for experimental validation and quantification of chemically relevant specific liver functions within the chambers, such as urea synthesis, gluconeogenesis, and ammonia metabolism.

Acknowledgments

This work was partially supported by Organogenesis, Inc., Canton, MA.

References

Arnaout, W. S., Moscioni, A. D., Barbour, R. L., and Demetriou, A. A., 1990, "Development of a Bioartificial Liver: Bilirubin Conjugation in Gunn Rats," *Journal of Surgical Research,* Vol. 48, pp. 379–382.

Asonuma, K., Gilbert, J. C., Stein, J. E., Takeda, T., and Vacanti, J. P., 1992, "Quantitation of Transplanted Hepatic Mass Necessary to Cure the Gunn Rat Model of Hyperbilirubinemia," *Journal of Pediatric Surgery,* Vol. 27, pp. 298–301.

Bader, A., Knop, E., Böker, K., Frühauf, N., Schüttler, W., Oldhafer, K., Burkhard, R., Pichlmayr, R., and Sewing, K.-F., 1995, "A Novel Bioreactor Design for *In Vitro* Reconstruction of *In Vivo* Liver Characteristics," *Artif. Organs,* Vol. 19, p. 365.

Balis, U. J., Behnia, K., Bhatia, S. N., Sullivan, S. L., Yarmush, M. L., and Toner, M., 1998, "Oxygen Consumption Characteristics of Porcine Hepatocytes," *Metabolic Engineering,* Vol. 1, p. 1.

Bejan, A., 1995, *Convection Heat Transfer,* 2nd ed., Wiley, New York.

Bhatia, S. N., Toner, M., Tompkins, E. G., and Yarmush, M. L., 1994, "Selective Adhesion of Hepatocytes on Patterned Surfaces," *Biochemical Engineering VIII,* Annals of the New York Academy of Sciences, Vol. 745, pp. 187–209.

Bhatia, S. N., Toner, M., Foy, B. D., Rotem, A., O'Neil, K. M., Tompkins, R. G., and Yarmush, M. L., 1996, "Zonal Liver Cell Heterogeneity: Effects of Oxygen on Metabolic Functions of Hepatocytes," *Cell Eng.,* Vol. 1, pp. 125–135.

Borel-Rinkes, I. H. M., Toner, M., Tompkins, R. G., and Yarmush, M. L., 1994, "An extracorporeal microscopy perfusion chamber for on-line studies of environmental effects on cultured hepatocytes." ASME JOURNAL OF BIOMECHANICAL ENGINEERING, Vol. 116: 135–139.

Britton, N. F., 1986, *Reaction-Diffusion Equations and Their Applications to Biology,* Academic Press, p. 202.

Campra, J. L., and Reynolds, T. B., 1988, "The Hepatic Circulation," in: M. Arias et al., eds., *The Liver Biology and Pathobiology,* Reven Press, New York, pp. 911–930.

Demetriou, A. A., Chowdury, N. M., Michalski, S., Whiting, J., Schechner, R., Feldman, D., Levenson, S. M., and Cowdury, J. R., 1986, "New Method of Hepatocyte Transplantation and Extracorporeal Liver Support," *Ann. Surg.,* Vol. 204, pp. 259–270.

Demetriou, A. A., Reisner, A., Sanchez, J., Levenson, S. M., Mocioni, A. D., and Chowdury, J. R., 1988, "Transplantation of Microcarrier-Attached Hepatocytes Into 90% Partially Hepatectomized Rats," *Hepatology,* Vol. 8, pp. 1006–1009.

Ellis, A. J., Hughes, R. D., Wendon, J. A., Dunne, J., Langley, P. G., Kelly, J. H., Gislason, G. T., Sussman, N. L., and Williams, R., 1996, "Pilot-Controlled Trial of the Extracorporeal Liver Assist Device in Acute Liver Failure," *Hepatology,* Vol. 24, pp. 1446–1451.

FIDAP, 1993, *Theory Manual,* Fluid Dynamics International, Evanston, IL, V. 7.0.

Foy, B. D., Rotem, A., Toner, M., Tompkins, R. G., and Yarmush, M. L., 1994, "A Device to Measure the Oxygen Uptake Rate of Attached Cells: Importance in Bioartificial Organ Design," *Cell Transplantation,* Vol. 3, pp. 515–527.

Frangos, J. A., McIntire, L. V., and Eskin, S. G., 1988, "Shear Stress Induced Simulation of Mammalian Cell Metabolism," *Biotechnology and Bioengineering,* Vol. 32, pp. 1053–1060.

Koike, M., Matsushita, M., Taguchi, K., and Uchino, J., 1996, "Function of Culturing Monolayer Hepatocytes by Collagen Gel Coating and Coculture With Nonparenchymal Cells," *Artif. Organs,* Vol. 20, pp. 186–192.

Goldstein, A. S., and DiMilla, P. A., 1997, "Application of Fluid Mechanics and Kinetic Models to Characterize Mammalian Cell Detachment in a Radial-Flow Chamber," *Biotechnology and Bioengineering,* Vol. 55, pp. 616–629.

Jauregui, H. O., Naik, S., Driscoll, J. L., Solomon, B. A., and Galletti, P. M., 1984, "Adult Rat Hepatocyte Cultures as the Cellular Component of an Artificial Hybrid Liver," in: *Biomaterials in Artificial Organs,* J. P. Paul, J. D. S. Gaylor, J. M. Courtney, and T. Gilchrest, eds. Macmillan Press, London.

Ledezma, G. A., and Bejan, A., 1997, "Optimal Spacing Between Staggered Vertical Plates in Natural Convection," ASME *Journal of Heat Transfer,* Vol. 119, pp. 700–708.

Nakata, K., Leong, G. F., and Brauer, R. W., 1960, "Direct Measurement of Blood Pressures in Minute Vessels of the Liver," *Am. J. Physiol.,* Vol. 6, pp. 1181–1188.

Nyberg, S. L., Shatford, R. A., Peshwa, M. V., White, J. G., Cerra, F. B., and Hu, W., 1993, "Evaluation of a Hepatocyte-Entrapment Hollow Fiber Bioreactor: A Potential Bioartificial Liver," *Biotechnol. Bioeng.,* Vol. 41, pp. 194–203.

Reddy, J. N., and Gartling, D. K., 1994, *The Finite Element Method in Heat Transfer and Fluid Mechanics,* CRC Press, Boca Raton, FL, pp. 158–159.

Rotem, A., Toner, M., Tompkins, R. G., and Yarmush, M. L., 1992, "Oxygen Uptake Rates in Cultured Rat Hepatocytes," *Biotechnology and Bioengineering,* Vol. 40, pp. 1286–1291.

Shnyra, A., Bocharov, A., Bochkova, N., and Spirov, V., 1991, "Bioartificial Liver Using Hepatocytes on Biosilon Microcarriers: Treatment of Chemically Induced Acute Hepatic Failure in Rats," *Artif. Organs,* Vol. 15, 189–197.

Stefanovich, P., Matthew, H. W. T., Toner, M., Tompkins, R. G., and Yarmush, M. L., 1996, "Extracorporeal Plasma Perfusion of Cultured Hepatocytes: Effect of Intermittent Perfusion on Hepatocyte Function and Morphology," *Journal of Surgical Research,* Vol. 66, pp. 57–63.

Sussman, N. L., and Kelly, J. H., 1996, "Artificial Liver Support," *Clinical and Investigative Medicine,* Vol. 19(5), pp. 393–399.

Taguchi, K., Matsushita, M., Takahashi, M., Uchino, J., 1996, "Function of Culturing Monolayer Hepatocytes by Collagen Gel Coating and Coculture With Nonparenchymal Cells," *Artif. Organs,* Vol. 20, pp. 178–185.

Takahashi, M., Matsue, H., Matsushita, M., Sato, K., Nishikawa, M., Koike, M., Noto, H., Nakajima, Y., Uchino, J., Komai, T., and Hashimura, E., 1992, "Does a Porcine Hepatocyte Hybrid Liver Prolong the Survival Time of Anhepatic Rabbits?" *ASAIO Journal,* Vol. 38, pp. M468–M472.

Truskey, G. A., and Pirone, J. S., 1990, "The Effect of Fluid Shear Stress Upon Cell Adhesion to Fibronectin-Treated Surfaces," *Journal of Biomedical Materials Research,* Vol. 24, pp. 1333–1353.

Uchino, J., Tsuburaya, T., Kumagai, F., Hase, T., Hamada, T., Komai, T., Funatsu, A., Hashimura, K., Nakamura, K., and Kon, T., 1988, "A Hybrid Bioartificial Liver Composed of Multiplated Hepatocyte Monolayers," *ASAIO Trans.,* Vol. 34, pp. 972–977.

Watanabe, F. D., Mullon, C. J., Hewitt, W. R., Arkadopoulos, N., Kahaku, E., Eguchi, S., Khalili, T., Arnaout, W., Shackleton, C. R., Rozga, J., Solomon, B., and Demetriou, A. A., 1997, "Clinical Experience With a Bioartificial Liver in the Treatment of Severe Liver Failure. A Phase I Clinical Trial," *Ann. Surg.,* Vol. 225, pp. 484–491.

Wu, F. J., Friend, J. R., Lazar, A., Mann, H. J., Remmel, R. P., Cerra, F. B., and Hu, W.-S., 1996, "Hollow Fiber Bioartificial Liver Utilizing Collagen-Entrapped Porcine Hepatocyte Spheroids," *Biotechnology and Bioengineering,* Vol. 52, pp. 34–44.

Yarmush, M. L., Dunn, J. C. Y., and Tompkins, R. G., 1992, "Assessment of Artificial Liver Support Technology," *Cell Transplantation,* Vol. 1, pp. 323–341.